Earth and Planetary Science Letters 457 (2017) 106–116

Contents lists available at ScienceDirect

Earth and Planetary Science Letters

www.elsevier.com/locate/epsl

Slab-derived halogens and noble gases illuminate closed system processes controlling volatile element transport into the mantle wedge

Masahiro Kobayashi [a,*], Hirochika Sumino [a,b], Keisuke Nagao [a,c], Satoko Ishimaru [d], Shoji Arai [e], Masako Yoshikawa [f], Tatsuhiko Kawamoto [g], Yoshitaka Kumagai [g,h], Tetsuo Kobayashi [i], Ray Burgess [j], Chris J. Ballentine [k]

[a] Geochemical Research Center, Graduate School of Science, The University of Tokyo, Tokyo 113-0033, Japan
[b] Department of Basic Science, Graduate School of Arts and Sciences, The University of Tokyo, Tokyo 153-8902, Japan
[c] Division of Polar Earth-System Sciences, Korea Polar Research Institute, Incheon 21990, South Korea
[d] Department of Earth and Environmental Science, Faculty of Science, Kumamoto University, Kumamoto 860-8555, Japan
[e] Department of Earth Sciences, Faculty of Science, Kanazawa University, Ishikawa 920-1192, Japan
[f] Institute for Geothermal Sciences, Graduate School of Science, Kyoto University, Oita 874-0903, Japan
[g] Institute for Geothermal Sciences, Graduate School of Science, Kyoto University, Kyoto 606-8502, Japan
[h] R&C IP Law Firm, Nakanoshima Mitsui Building 3-3, Osaka 530-0005, Japan
[i] Department of Earth and Environmental Sciences, Graduate School of Science and Engineering, Kagoshima University, Kagoshima 890-0065, Japan
[j] School of Earth and Environmental Sciences, The University of Manchester, Manchester M13 9PL, United Kingdom
[k] Department of Earth Sciences, University of Oxford, Oxford OX1 3AN, United Kingdom

ARTICLE INFO

Article history:
Received 20 May 2016
Received in revised form 23 September 2016
Accepted 11 October 2016
Available online 25 October 2016
Editor: B. Marty

Keywords:
halogen
noble gas
subduction zone
volatile recycling
mantle peridotite
slab fluids

ABSTRACT

Halogen and noble gas systematics are powerful tracers of volatile recycling in subduction zones. We present halogen and noble gas compositions of mantle peridotites containing H_2O-rich fluid inclusions collected at volcanic fronts from two contrasting subduction zones (the Avacha volcano of Kamchatka arc and the Pinatubo volcano of Luzon arcs) and orogenic peridotites from a peridotite massif (the Horoman massif, Hokkaido, Japan) which represents an exhumed portion of the mantle wedge. The aims are to determine how volatiles are carried into the mantle wedge and how the subducted fluids modify halogen and noble gas compositions in the mantle. The halogen and noble gas signatures in the H_2O-rich fluids are similar to those of marine sedimentary pore fluids and forearc and seafloor serpentinites. This suggests that marine pore fluids in deep-sea sediments are carried by serpentine and supplied to the mantle wedge, preserving their original halogen and noble gas compositions. We suggest that the sedimentary pore fluid-derived water is incorporated into serpentine through hydration in a closed system along faults at the outer rise of the oceanic, preserving Cl/H_2O and $^{36}Ar/H_2O$ values of sedimentary pore fluids. Dehydration–hydration process within the oceanic lithospheric mantle maintains the closed system until the final stage of serpentine dehydration. The sedimentary pore fluid-like halogen and noble gas signatures in fluids released at the final stage of serpentine dehydration are preserved due to highly channelized flow, whereas the original Cl/H_2O and $^{36}Ar/H_2O$ ratios are fractionated by the higher incompatibility of halogens and noble gases in hydrous minerals.

1. Introduction

Water is one of the most important volatiles in many processes studied in earth sciences. It is a major component degassed from the Earth's interior through volcanism at mid-ocean ridges, hot spots, and arcs and is returned via subduction processes. Hydrous minerals in subducting slabs transport water by incorporating it as OH groups. The water is released from the subducting slabs to the mantle wedge through dehydration of those hydrous minerals. Even a relatively small amount of water may result in major changes to the chemical and physical properties of mantle

* Corresponding author.
E-mail addresses: kobayashi@eqchem.s.u-tokyo.ac.jp (M. Kobayashi), sumino@igcl.c.u-tokyo.ac.jp (H. Sumino), nagao@kopri.re.kr (K. Nagao), ishimaru@sci.kumamoto-u.ac.jp (S. Ishimaru), ultrasa@staff.kanazawa-u.ac.jp (S. Arai), masako@bep.vgs.kyoto-u.ac.jp (M. Yoshikawa), kawamoto@bep.vgs.kyoto-u.ac.jp (T. Kawamoto), yoshitaka.kumagai@rc-iplaw.com (Y. Kumagai), koba01@cma.bbiq.jp (T. Kobayashi), ray.burgess@manchester.ac.uk (R. Burgess), chris.ballentine@earth.ox.ac.uk (C.J. Ballentine).

http://dx.doi.org/10.1016/j.epsl.2016.10.012

rocks, influencing mineral phase assemblages, melting temperatures, viscosities, seismic wave velocities, and electrical conductivities (Bolfan-Casanova, 2005; Kawamoto et al., 2015). Volcanism and seismicity associated with subduction zones is also linked to the dehydration processes and release of water from the subducting slabs (Mitsui and Hirahara, 2009; Tatsumi, 1989), although the detail of hydrous mineral and water release mass balance remains debated (e.g., Iwamori, 2007; van Keken et al., 2011; Wada et al., 2012).

Concentrations of heavy halogens (chlorine, bromine, and iodine) and noble gases in the Earth's surface reservoirs are significantly higher than in the mantle. For example, ^{36}Ar and chlorine concentrations in the depleted mantle are 6×10^{-11} ccSTP ^{36}Ar/g (Holland and Ballentine, 2006) and <6 ppm Cl (John et al., 2011) respectively, whereas in seawater they are orders of magnitude higher at 1.3×10^{-6} ccSTP ^{36}Ar/g (Ozima and Podosek, 2002) and 19400 ppm Cl (Bruland and Lohan, 2006). Noble gases are strongly partitioned into gas- and fluid-phases relative to minerals (Ozima and Podosek, 2002) and heavy halogens are also strongly partitioned into aqueous fluids (Bureau et al., 2000, 2016). The large contrast in concentrations between the surface and interior of the Earth means that halogens and noble gases are potentially powerful tracers of slab-derived aqueous fluids in the mantle. Furthermore, the distinct elemental and/or isotopic compositions of halogens and noble gases (e.g., Ballentine and Holland, 2008; Chavrit et al., 2016; Holland and Ballentine, 2006; John et al., 2011; Kendrick et al., 2011, 2012, 2013, 2015; Ozima and Podosek, 2002; Porcelli and Ballentine, 2002; Staudacher and Allègre, 1988; Sumino et al., 2010) can be used to reveal the origin and/or the subduction path of subducted water.

Subducted materials in slabs are recycled into the deep mantle, but volatiles including halogens and noble gases are often assumed to be returned to the surface through arc volcanism with little, if any transferred to the deep mantle (Staudacher and Allègre, 1988). Despite this "subduction barrier", the ratios of non-radiogenic isotopes of heavy noble gases (argon, krypton, and xenon) in the convecting mantle are similar to those of seawater and distinct from other subducted materials (Ballentine and Holland, 2008; Holland and Ballentine, 2006). In addition, evidence for subducted noble gases in mantle peridotites has been found from many regions (e.g., Hopp and Ionov, 2011; Matsumoto et al., 2001; Sumino et al., 2010). Evidence of halogen recycling into the deep mantle has also been found in plume related volcanic rocks (e.g., John et al., 2010). Sumino et al. (2010) studied halogens and noble gases in mantle wedge peridotites from the Higashi-akaishi peridotite body in the Sanbagawa metamorphic belt, Shikoku Island, Japan, in which slab-derived H_2O-rich fluids were trapped just above the subducting slab at ≥100 km depth. These peridotites contain noble gas compositions similar to those of seawater, however their high I/Cl values indicate the presence of a marine sedimentary pore fluid. This aqueous fluid originates as seawater trapped in the pores of marine sediments that is subsequently enriched in iodine by the decomposition of organic materials in the sediments (e.g., Fehn et al., 2006). Similar sedimentary pore fluid-like signatures have also been found in fluid inclusions in a quartz vein in metapelites from the Besshi, Sanbagawa metamorphic belt (Sumino et al., 2011). These fluid inclusions are considered to represent fluids captured during the prograde path, or near the peak metamorphic stage of subduction (Yoshida and Hirajima, 2012). John et al. (2011) and Kendrick et al. (2011, 2013) have shown that serpentinites in the oceanic lithosphere contain substantial amounts of sedimentary pore fluid-like noble gases and halogens, suggesting that serpentine may be an important carrier of pore fluid-derived water.

In this study, we report halogen and noble gas compositions in mantle xenoliths collected at the volcanic fronts from two different subduction zones (the Kamchatka and Luzon arcs), and orogenic peridotites from a peridotite massif (the Horoman peridotite massif, Japan), that latter represents a portion of the mantle wedge infiltrated with slab-derived H_2O–CO_2 rich fluids. We consider the extent to which the mantle wedge signature is preserved in orogenic peridotite samples that are subject to modification processes during exhumation. In contrast, the rapid ascent of mantle xenoliths has favored retention of a direct record of metasomatic processes in the mantle wedge. We discuss how slab-derived fluids are transferred into the mantle wedge and how they modify the mantle halogen and noble gas compositions.

2. Samples

Mantle xenoliths are from the Avacha volcano, the Kamchatka peninsula, Russia and the Pinatubo volcano, Luzon island, in the Philippines. These volcanoes are located at the volcanic fronts of the Kamchatka and Luzon arcs, respectively. The old and cold Pacific plate is subducting beneath the Avacha volcano (Minster et al., 1974), whereas the young and hot South China Sea plate is subducting beneath the Pinatubo volcano (Briais et al., 1993). The xenolith lithologies are spinel-harzburgites with textures and chemical compositions that reflect differing extents of metasomatism (Ishimaru and Arai, 2009; Ishimaru et al., 2007; Kawamoto et al., 2013; Yoshikawa et al., 2016). There are two subtypes of Avacha peridotites characterized by either the presence or absence of fine-grained (<100 μm) olivine domains (Arai et al., 2003). All Avacha samples examined in this study are the coarse-grained type, except for Avx-1, which contains domains of fine-grained olivine (Avx-1 F-part). One Pinatubo sample (P2) contains fine-grained domains, whereas the other sample (P3) is of the coarse-grained type. The Avacha and Pinatubo harzburgites contain H_2O-rich fluid inclusions (Fig. 1) having salinities of 5.1 ± 1.0 wt% NaCl-equivalent for Pinatubo (Kawamoto et al., 2013) and 2–8 wt% NaCl-equivalent for Avacha (Ishimaru, unpublished results). Hopp and Ionov (2011) reported atmospheric noble gases present in fluid inclusions in Avacha xenoliths, arguing for their incorporation into the mantle wedge via slab-derived fluids. Hereafter we refer to atmospheric noble gases as those that show isotopic ratios similar to the air (elemental ratios can vary from those in the air).

The orogenic peridotite studied is from the Horoman peridotite massif in Hokkaido, Japan. The sample is a fragment of a peridotite block from which a powder has previously been prepared and distributed by the Geological Survey of Japan as the geochemical reference material JP-1. Hereafter we refer to this sample as JP-1. Although JP-1 is described as a dunite by Imai et al. (1995), it consists of olivine, orthopyroxene, clinopyroxene, and chromian spinel indicating it more appropriately classified as a harzburgite (Appendix A). Hirai and Arai (1987) have suggested that the Horoman peridotite massif represents an exhumed portion of the mantle wedge infiltrated with H_2O–CO_2 rich fluids, the latter based on finding relic fluid inclusions in Horoman dunites. A mantle wedge origin is supported by trace element patterns and Nd–Sr isotopes of Horoman harzburgites and lherzolites (Yoshikawa and Nakamura, 2000). Horoman lherzolites and harzburgites including JP-1 have atmospheric noble gas compositions (Ikeda et al., 2001; Matsumoto et al., 2001; Miura and Nagao, 1991) and Matsumoto et al. (2001) showed that the atmospheric ^{36}Ar concentrations correlate with mantle-derived ^{3}He, indicating that the atmospheric noble gases are a recycled component derived from the subducting slab.

3. Experimental methods

The peridotite samples were coarsely crushed into 0.5–2 mm mineral grains (or aggregates of fine-grained minerals in the case

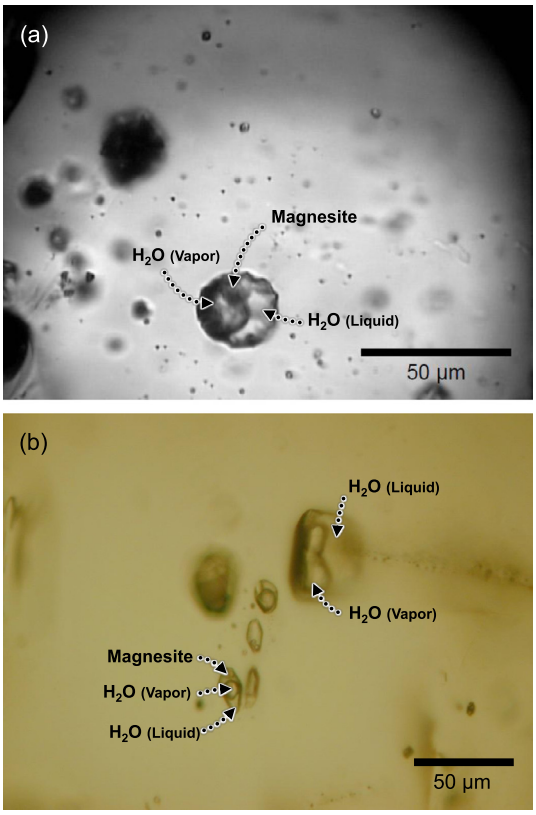

Fig. 1. Photomicrographs of fluid inclusions in olivine. (a) Sample #629 from the Avacha volcano. (b) Sample P3 from the Pinatubo volcano (Kawamoto et al., 2013). The fluid inclusions are distributed as isolated small clusters or trails. The fluid inclusions are composed mainly of liquid H_2O, magnesite, and a vapor H_2O bubble. Some of the vapor bubbles contain CO_2. Scale bars are 50 μm.

of Avx-1 F-part) and leached with 1N nitric acid. Olivine separates were obtained from the Pinatubo harzburgites by hand-picking under a binocular microscope. We determined halogens using neutron irradiation and noble gas mass spectrometry (Böhlke and Irwin, 1992; Johnson et al., 2000; Kendrick, 2012; Ruzié-Hamilton et al., 2016; Turner, 1965). In this method, halogens (chlorine, bromine, and iodine) and other elements (potassium, calcium, barium, and uranium) are converted to corresponding isotopes of argon, krypton, and xenon by neutron irradiation in a nuclear reactor. Since halogens have relatively high cross-sections for neutron capture, and the sensitivity of noble gas mass spectrometry is high, trace amounts of halogens in a mantle peridotite sample can be determined.

The peridotite samples, each weighing ~50 mg, were wrapped in aluminum foil and placed in aluminum cans. Neutron irradiation was carried-out in position HR of Japan Research Reactor-3 (JRR-3), Japan Atomic Energy Agency for 24–48 h. Thermal and fast neutron fluences were determined using the Hb3gr hornblende monitor sample encapsulated in the aluminum can with the peridotite samples (Appendix B). During previous irradiations in position HR of JRR-3, the Shallowater meteorite had been irradiated in order to evaluate additional production of noble gas isotopes from resonances of epithermal neutrons (e.g., Johnson et al., 2000), which was found to be negligible. With the exception of samples JP-1 #a and #b, the calcium-derived ^{37}Ar (half-life of 35 days) had decayed before the samples were analyzed. Interference from calcium-derived ^{39}Ar, ^{38}Ar, and ^{36}Ar is considered to be of minor importance because only small amounts of calcium-derived argon isotopes are estimated to have been produced based on their low production rates determined in previous irradiations in position HR of JRR-3, and because the calcium concentrations of the samples are relatively low (<1.3 wt% of CaO; Imai et al., 1995; Ishimaru et al., 2007).

Neutron-irradiated samples were analyzed using a noble gas analysis system modified from that described by Ebisawa et al. (2004). Noble gases were extracted by sample fusion and stepwise crushing methods. In both methods, samples were initially baked-out under vacuum at 200 °C overnight. The bulk halogen compositions were determined by fusing the samples at 1800 °C for 30 min in a W-coil furnace. Noble gases from JP-1 #a and #b were extracted by stepped heating from 700 to 1800 °C using 9 steps. A separate aliquot of each sample was crushed using a hydraulic press, in order to selectively release noble gases from fluid inclusions (e.g., Kurz, 1986). Extracted gases are purified by Ti–Zr getters, separated into argon, krypton, and xenon fractions using a porous sintered stainless steel filter element under cryogenic temperature control, and then each fraction was admitted into a modified VG3600 mass spectrometer.

Helium, neon, and argon isotope ratios were determined on 0.4–1 g samples of unirradiated peridotites using techniques described in Sumino et al. (2001). Each sample was heated at 800 °C for 30 min before stepwise crushing, in order to reduce adsorbed atmospheric noble gases. Isotope ratios of krypton and xenon were not measured in this study since their ratios are often dominated by atmospheric components in subduction zones and atmospheric xenon isotope ratios were reported previously for Avacha xenoliths (Hopp and Ionov, 2011).

4. Results

4.1. Halogen composition

The halogen data are given in Table 1 and Supplementary Table S1. During stepped crushing, the proportion of noble gases released from fluid inclusions relative to other potential sites (e.g., lattice or grain boundaries) may change as the intensity of crushing increases (e.g., Hilton et al., 1993). However, the compositions obtained for crushing steps from each sample (Supplementary Table S1) indicate that noble gases are released mainly from fluid inclusions, and that the release was primarily of a single compositional type. Despite only relic fluid inclusions being observed in Horoman peridotites (Hirai and Arai, 1987), significant amounts and constant elemental ratios of halogens were obtained during stepped crushing, suggesting that these inclusions still contain aqueous fluids.

All peridotite samples are strongly enriched in iodine with I/Cl and Br/Cl ratios similar to sedimentary pore fluids and serpentinites (Fig. 2). Contributions from mid-ocean ridge basalt (MORB) source mantle and altered oceanic crust (seafloor basalts and metagabbros) are of minor importance. Whereas the halogen compositions of fluids in Pinatubo harzburgites and Horoman peridotites overlap with those of sedimentary pore fluids, the fluids in Avacha harzburgites deviate from the sedimentary pore fluid trend towards higher I/Cl values. Such iodine enrichment was observed previously in mantle wedge peridotites from Higashi-akaishi (Sumino et al., 2010) and forearc serpentinites from the Mariana arc (Kendrick et al., 2013). Most of the samples show slightly lower I/Cl and Br/Cl ratios during heating compared to crushing, suggesting the presence of an additional halogen host phase(s) in the bulk rock.

4.2. Noble gas composition

The isotopic ratios of neon and argon (Supplementary Table S2) are dominated by atmospheric components, similar to the findings of previous studies of Avacha and Horoman peridotites (Hopp and Ionov, 2011; Ikeda et al., 2001; Matsumoto et al., 2001;

Table 1
Concentrations and elemental ratios of halogens and Cl/^{40}Ar* ratios.

Sample	Extraction	Cl (ppm)	Br (ppb)	I (ppb)	Br/Cl (10^{-3} mol/mol)	I/Cl (10^{-6} mol/mol)	Cl/^{40}Ar* (10^{4} mol/mol)
Avacha							
#10	Heating	7.48 (62)	23.1 (19)	17.6 (18)	1.37 (16)	658 (86)	10.7 (15)
	Crushing	4.19 (21)	15.39 (78)	12.72 (80)	1.63 (12)	849 (68)	5.15 (36)
#122	Heating	11.92 (98)	46.2 (39)	40.8 (42)	1.72 (20)	957 (126)	1.10 (13)
	Crushing	2.57 (13)	11.67 (59)	11.64 (72)	2.02 (15)	1267 (102)	0.799 (61)
#187	Heating	4.20 (35)	13.0 (11)	10.3 (11)	1.38 (16)	685 (90)	9.4 (19)
	Crushing	1.364 (72)	4.92 (26)	4.37 (29)	1.60 (12)	896 (76)	6.9 (15)
#203	Heating	12.1 (10)	34.7 (29)	12.2 (12)	1.27 (15)	280 (36)	2.31 (30)
	Crushing	2.15 (11)	9.62 (51)	6.97 (47)	1.99 (15)	906 (77)	0.899 (72)
#629	Heating	14.7 (12)	39.9 (33)	13.6 (14)	1.20 (14)	257 (34)	4.14 (56)
	Crushing	1.757 (93)	7.64 (41)	3.61 (24)	1.93 (15)	575 (49)	0.916 (80)
#729	Heating	2.80 (23)	10.89 (91)	6.59 (67)	1.73 (20)	658 (86)	1.81 (20)
	Crushing	1.075 (57)	3.97 (20)	2.69 (17)	1.64 (12)	699 (58)	1.48 (11)
F1	Heating	6.93 (57)	17.3 (14)	15.3 (15)	1.107 (13)	616 (80)	10.1 (13)
	Crushing	5.72 (30)	18.21 (99)	10.78 (71)	1.41 (11)	527 (45)	9.8 (10)
Avx1 C-part	Heating	7.78 (64)	17.8 (15)	11.6 (12)	1.01 (12)	417 (55)	10.4 (13)
	Crushing	1.111 (60)	4.41 (24)	4.53 (30)	1.76 (13)	1139 (97)	2.94 (30)
Avx1 F-part	Heating	3.15 (26)	8.30 (69)	7.53 (76)	1.17 (14)	668 (87)	3.71 (58)
	Crushing	0.620 (30)	2.56 (13)	2.43 (15)	1.84 (13)	1095 (85)	1.76 (23)
Avx33	Heating	10.00 (83)	30.8 (26)	16.0 (16)	1.37 (16)	448 (59)	10.0 (12)
	Crushing	2.73 (15)	10.59 (58)	10.50 (71)	1.72 (13)	1075 (94)	2.38 (18)
Pinatubo							
P2	Heating	12.77 (80)	36.7 (23)	7.15 (62)	1.27 (11)	156 (17)	10.8 (29)
	Crushing	2.49 (11)	9.73 (43)	2.45 (15)	1.73 (11)	275 (20)	5.43 (47)
P2 olivine	Heating	12.41 (78)	47.6 (30)	10.28 (89)	1.70 (15)	231 (25)	8.3 (19)
	Crushing	5.73 (24)	21.69 (89)	5.58 (31)	1.68 (10)	272 (19)	5.58 (57)
P3	Heating	11.54 (72)	44.8 (28)	11.6 (10)	1.72 (5)	281 (30)	9.0 (28)
	Crushing	3.37 (13)	14.25 (57)	2.59 (15)	1.87 (11)	215 (15)	4.78 (82)
P3 olivine	Heating	16.3 (10)	64.6 (41)	15.1 (13)	1.76 (16)	259 (28)	8.8 (17)
	Crushing	2.524 (95)	10.00 (38)	2.71 (14)	1.758 (94)	300 (19)	6.55 (48)
Horoman							
JP-1 #a	Heating	9.94 (25)	23.04 (58)	3.139 (87)	1.028 (36)	88.2 (33)	10.60 (45)
JP-1 #b	Heating	11.22 (36)	28.40 (83)	4.32 (12)	1.123 (49)	107.7 (46)	16.3 (13)
JP-1 #c	Crushing	1.342 (50)	6.30 (24)	1.357 (58)	2.08 (11)	282 (16)	6.02 (56)
JP-1 #d	Crushing	0.983 (37)	4.93 (19)	1.003 (40)	2.22 (12)	285 (16)	12.5 (12)
JP-1 #e	Crushing	0.511 (19)	2.337 (88)	0.602 (31)	2.03 (11)	329 (21)	2.44 (35)
JP-1 #f	Crushing	0.521 (19)	2.064 (78)	0.693 (36)	1.757 (93)	371 (24)	3.93 (65)

Errors are given as least significant figures in brackets at a 1σ level of confidence. ^{40}Ar* is radiogenic ^{40}Ar, defined as $^{40}Ar^* = \{(^{40}Ar/^{36}Ar)_{measured} - (^{40}Ar/^{36}Ar)_{air}\} \times {}^{36}Ar$, where $(^{40}Ar/^{36}Ar)_{air} = 296$ (Ozima and Podosek, 2002). The data obtained by crushing represents the total release obtained by summing all steps. The data of JP-1 #a and #b are the total amounts obtained by summing all heating steps. The data for individual crushing and heating steps are given in Supplementary Table S1.

Miura and Nagao, 1991). Note that we refer to 'atmospheric noble gases' as those that show isotopic ratios similar to the air (elemental ratios may be different from those of the air). The weighted mean ^{3}He/^{4}He values (Supplementary Table S2) are: 7.724 ± 0.019 Ra (1 Ra = atmospheric ratio of 1.399×10^{-6}; Ozima and Podosek, 2002) for Avacha; 7.478 ± 0.023 Ra for Pinatubo; and 8.726 ± 0.038 Ra for Horoman (errors are 1σ). These ratios are consistent with the ^{3}He/^{4}He value of MORB (8.8 ± 2.1 Ra; Graham, 2002) and are uniform in samples from each locality. The ^{3}He/^{4}He ratios of Horoman samples are consistent with those reported by previous studies (7.6–9.2 Ra; Ikeda et al., 2001; Matsumoto et al., 2001; Miura and Nagao, 1991), though a slightly wider range of between 5.2 and 8.1 Ra was obtained for Avacha xenoliths by Hopp and Ionov (2011).

The ^{4}He/^{40}Ar* ratios (Supplementary Table S2; $^{40}Ar^* = \{(^{40}Ar/^{36}Ar)_{measured} - (^{40}Ar/^{36}Ar)_{air}\} \times {}^{36}Ar$) are 0.3–3.4 for Avacha, 1.0–3.4 for Pinatubo, and 20 for Horoman. The range of values from Avacha and Pinatubo harzburgites overlaps with the ^{4}He/^{40}Ar* production ratio in the MORB mantle of 1.6–4.2 (Graham, 2002). Although some samples show lower ^{4}He/^{40}Ar* than the MORB mantle, similarly low ratios were reported for Avacha xenoliths (0.16–0.90; Hopp and Ionov, 2011) and for mantle-derived samples from other subduction zones (e.g., Yamamoto et al., 2009). Horoman harzburgite sampled close to the locality of JP-1 gave a high ^{4}He/^{40}Ar* ratio (12.8), whereas the values for other harzburgites (1.5–4.5) are consistent with the mantle production ratio (1.6–4.2) (Matsumoto et al., 2001). ^{4}He/^{40}Ar* ratios obtained by fusing samples gave values of 20–50 for JP-1 but only 3–4 for Horoman lherzorite and harzburgite (Ikeda et al., 2001; Matsumoto et al., 2001; Miura and Nagao, 1991).

In a 3D plot of ^{22}Ne/^{36}Ar, ^{84}Kr/^{36}Ar, and ^{132}Xe/^{36}Ar ratios (Fig. 3), data for Avacha and Pinatubo harzburgites plot between seawater and air compositions. Previously Hopp and Ionov (2011) obtained similar noble gas elemental ratios for Avacha peridotites and their data are shown for comparison in Fig. 3. The Horoman peridotite exhibits slightly higher ^{84}Kr/^{36}Ar and ^{132}Xe/^{36}Ar ratios than seawater.

5. Discussion

5.1. Noble gases in mantle wedge peridotites

Noble gas data shown in the 3D diagram of ^{22}Ne/^{36}Ar–^{84}Kr/^{36}Ar–^{132}Xe/^{36}Ar (Fig. 3) indicate overwhelming contributions from air and air-saturated seawater to Avacha and Pinatubo harzburgites, however data show a slight deviation from the mixing line between air and seawater towards high Kr/Ar and Xe/Ar and/or high Ne/Ar values. This plot also indicates a negligible contribution of altered oceanic crust or marine sediment-related noble gases. Deviation from the air–seawater mixing cannot be explained by mantle-derived noble gases because the atmospheric neon isotope ratios of the samples indicates limited contribution from mantle-derived noble gases except for helium and ^{40}Ar* (Supplementary Table S2). Mass-dependent fractionation can account for

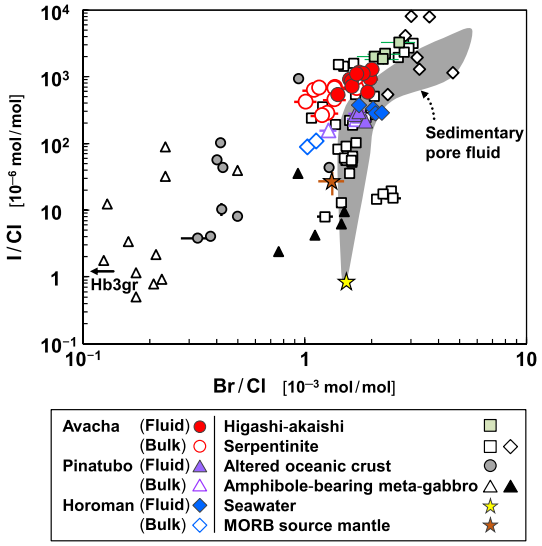

Fig. 2. I/Cl versus Br/Cl for Avacha, Pinatubo and Horoman samples. Fluid and Bulk refer to crushing and heating data, respectively. Errors are 1σ. The halogen composition of Hb3gr hornblende plots off the figure as indicated by the arrow (Br/Cl = 0.0047–0.13 × 10^{-3} mol/mol and I/Cl = 1.1–9.1 × 10^{-6} mol/mol). Data sources: Higashi-akaishi peridotite from Sanbagawa metamorphic belt and sedimentary pore fluids (Sumino et al., 2010 and references therein), serpentinites from the oceanic lithosphere (open squares) and forearc (open diamonds) (John et al., 2011; Kendrick et al., 2011, 2013), seawater (Bruland and Lohan, 2006), MORB source mantle (Kendrick et al., 2012), altered oceanic crust older than 100 Ma (Chavrit et al., 2016), amphiboles in meta-gabbros (open triangles) and relict minerals and quartz-epidote veins in meta-gabbros (black triangles) (Kendrick et al., 2015), and Hb3gr hornblende (Kendrick, 2012; this study, see Supplementary Table S1). The halogen ratios reported by Kendrick et al. (2011, 2012) and Kendrick (2012) were recalculated using revised values for scapolite monitors (Kendrick et al., 2013).

increasing Kr/Ar and Xe/Ar values, however this process is ruled-out because it should lead to Ne/Ar ratios lower than the air value, and this is the opposite to that observed in Fig. 3. The origin of the air-like component is unclear at present; however it is possible that some over-pressured fluid inclusions ruptured during ascent in the crust or during eruption, and were subsequently refilled with air-derived noble gases that penetrated along microfractures before resealing of the inclusions (Ballentine and Barfod, 2000). If the air-like component was incorporated into the samples close to and/or at the Earth's surface, then the original noble gas elemental ratios of the slab-derived fluids in Avacha and Pinatubo harzburgites were seawater-like.

The $^{84}Kr/^{36}Ar$ and $^{132}Xe/^{36}Ar$ ratios of the Horoman peridotite that are slightly higher than seawater cannot be explained by simple mixing between seawater and unfractionated air (Fig. 3). The direction of the deviation from seawater could result from a contribution from altered oceanic crust; however, this is not apparent in the halogen elemental ratios (Fig. 2). Based upon petrological studies of Horoman peridotites, it has been argued that, prior to being exhumed to the surface, they experienced more complicated processes compared to Avacha and Pinatubo harzburgites, including partial melting and crystallization during formation of the peridotite complex (e.g., Takahashi, 1992). It is possible that the initial seawater-like noble gas elemental ratios underwent fractionation during these processes.

The seawater-derived noble gases cannot account for the presence of MORB-like helium in the fluid inclusions (Supplementary Table S2). Because helium is scarce in surface reservoirs and relatively enriched in the mantle, MORB-like helium in the fluid inclusions is most likely acquired from the ambient mantle by the slab-derived fluids. The lower $^{3}He/^{4}He$ values of previously studied Avacha xenoliths were considered to be a feature of the continental lithospheric mantle beneath the Avacha volcano reflecting a higher

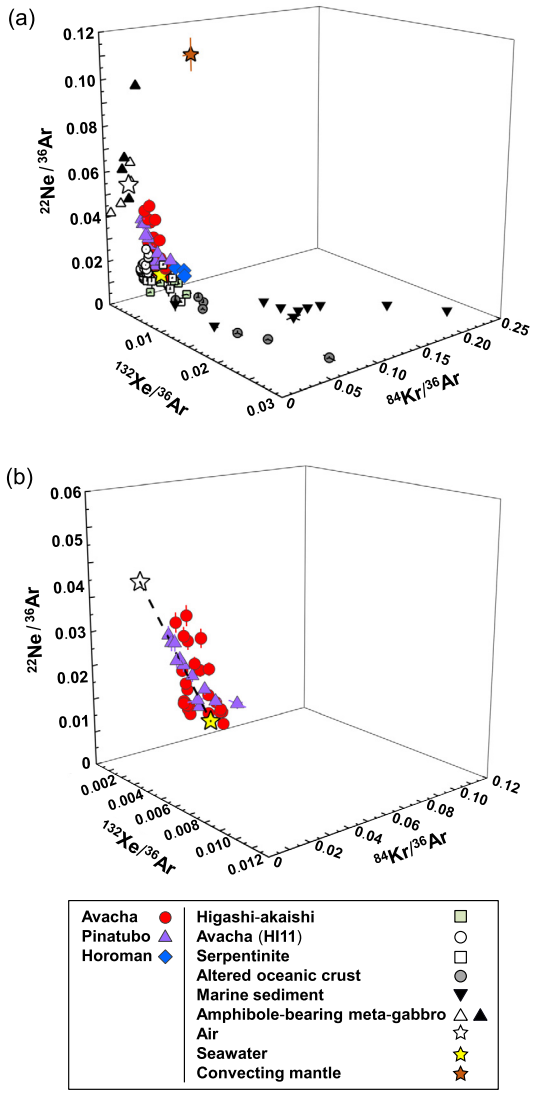

Fig. 3. $^{22}Ne/^{36}Ar$ versus $^{84}Kr/^{36}Ar$ versus $^{132}Xe/^{36}Ar$. (b) is a magnification of (a) including only Avacha and Pinatubo data which lie close to a mixing line between air and seawater (dashed line). Errors are 1σ. Data sources: seawater at 0 °C and air (Ozima and Podosek, 2002), the convecting mantle (Holland and Ballentine, 2006), Higashi-akaishi peridotites from Sanbagawa metamorphic belt (Sumino et al., 2010), Avacha sample HI11 (Hopp and Ionov, 2011), marine sediments (Matsuda and Nagao, 1986; Staudacher and Allègre, 1988), serpentinites (Kendrick et al., 2011, 2013), altered oceanic crust (Chavrit et al., 2016; Staudacher and Allègre, 1988), and amphiboles in meta-gabbros (open triangles) and relict minerals and quartz-epidote veins in meta-gabbros (black triangles) (Kendrick et al., 2015).

(U+Th)/^{3}He ratio than the MORB source due to ancient metasomatism (Hopp and Ionov, 2011). The fluid inclusions in each sample studied here show identical $^{3}He/^{4}He$ ratios during stepped crushing (weighted RSD = 0.5–1%), whereas the $^{3}He/^{4}He$ ratios reported by Hopp and Ionov (2011) show a greater range (weighted RSD = 4–14%). The larger variation in the Hopp and Ionov (2011) helium isotope data may indicate that two or more helium components are present in the mantle beneath the Avacha volcano, although only one component is observed in our study.

Because there is no $^{40}Ar^{*}$ in seawater, the $^{40}Ar^{*}$ in the fluid inclusions can also be attributed to an ambient mantle source. Contributions of $^{40}Ar^{*}$ from oceanic crust and/or sediment can potentially explain the low $^{4}He/^{40}Ar^{*}$ ratios of Avacha and Pinatubo harzburgites, however this is rejected on the basis that it is inconsistent with the noble gas data discussed earlier (Fig. 3). $^{4}He/^{40}Ar^{*}$ ratios can be fractionated by different processes in the mantle. Sol-

ubility controlled and kinetic fractionation during partial melting and fluid exsolution are processes that can lead to low $^{4}He/^{40}Ar^{*}$ ratios (Burnard, 2004; Heber et al., 2007; Hopp and Ionov, 2011; Yamamoto et al., 2009). The mantle beneath arcs has experienced several melt extraction events and as a response the mantle wedge will develop low $^{4}He/^{40}Ar^{*}$ ratios.

5.2. Halogens in the mantle wedge peridotites

The halogen elemental ratios plot on or close to data for marine sedimentary pore fluids and serpentinites (Fig. 2). Avacha harzburgites show a slight elevation of I/Cl above the marine pore fluid range, similar to the fluids analyzed in Higashi-akaishi peridotites studied previously (Sumino et al., 2010) and serpentinites from the Mariana forearc (Kendrick et al., 2013), where iodine enrichment of marine pore fluid was attributed to breakdown of organic matter in sediments. The interpretation for a sedimentary pore fluid origin for halogens is entirely consistent with the noble gas data presented in section 5.1. We argue that the consistency is strong evidence that the halogen and noble gas signatures derived from sedimentary pore fluid have been preserved during the subduction processes without significant fractionation.

Fig. 2 shows that for most samples the bulk (heating) Br/Cl and I/Cl ratios are lower than the fluid (crushing) values (Table 1), which suggests that bulk rocks contain an additional chlorine-bearing phase(s). Amphibole is reported to be present in the peridotite samples analyzed (Arai and Takahashi, 1989; Ishimaru et al., 2007; Kawamoto et al., 2013), and this mineral may potentially contain relatively high chlorine concentrations associated with low Br/Cl and I/Cl ratios (Fig. 2). The chlorine concentrations of amphibole in the Pinatubo and Avacha xenoliths determined by EPMA (Appendix C) are low ($\leq$400 ppm) or below detection limit (130 ppm). The low chlorine concentration in amphibole and low modal amount of this mineral in the peridotite samples ($<$2.5%, mostly $<$1.0% in the Avacha harzburgites; Ishimaru et al., 2007) require the presence of an additional chlorine-bearing phase(s). Silicate glass containing $>$1000 ppm of chlorine (Appendix C), present in some Avacha xenoliths (Ishimaru et al., 2007; Ishimaru and Arai, 2009), is likely to have low Br/Cl and I/Cl ratios. Irrespective of minor halogen variation, the bulk compositions remain overwhelmingly dominated by a marine sedimentary pore fluid signature carried by the fluid. It is notable that olivine separates yield comparable I/Cl and Br/Cl ratios during heating and crushing (Table 1) indicating that fluids are the only source of halogens contained in this mineral phase.

5.3. Sedimentary pore fluid-like signatures in the mantle wedge peridotites

Sedimentary pore fluid-like halogen and noble gas signatures are present in both mantle xenoliths and orogenic peridotites from subduction zones. This indicates that these signatures are an intrinsic feature of the mantle wedge and not the result of alteration processes such as interaction of the host magmas with the xenoliths or shallow level contamination during exhumation. These signatures are present in two different subduction zones, which show a strong contrast in the thermal structures of their subducting slabs (van Keken et al., 2011). This suggests that subduction of sedimentary pore fluid-derived noble gases and halogens is a ubiquitous phenomenon in modern subduction zones and that its influence is not necessarily restricted to the wedge-slab interface (Sumino et al., 2010) and significantly extends into the mantle wedge.

Despite having distinctly different solubilities in H_2O-rich fluids and silicate minerals, noble gases and halogens retain their primary sedimentary pore fluid signature and are not therefore decoupled during volatile cycling in the mantle wedge. This implies sedimentary pore fluid-derived water may be subducted and supplied to the mantle wedge directly as a free fluid phase, trapped either as fluid inclusions and/or as fluids in the pore spaces of a slab, or that they are being transported by a hydrous phase capable of retaining the primary signature. Subduction of a free fluid phase is considered unlikely because the pore spaces of sediments collapse at shallow subduction levels due to compaction, resulting in an insignificant flux of water into the mantle by this process (e.g., Jarrard, 2003). However, serpentinites are known to show sedimentary pore fluid-like signatures, and it has been suggested that serpentine minerals are the carrier phase of halogens (John et al., 2011; Kendrick et al., 2011, 2013).

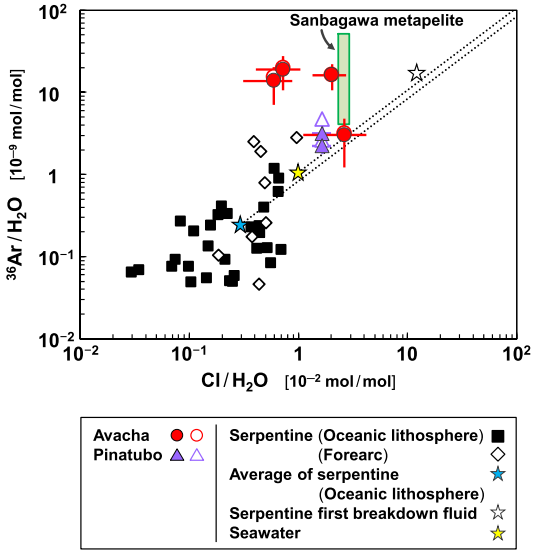

Fig. 4. $^{36}Ar/H_2O$ versus Cl/H_2O. For Avacha and Pinatubo, solid symbols represent data corrected for ^{36}Ar contamination from air, based on the $^{22}Ne/^{36}Ar$ ratios, open symbols are uncorrected values. Dashed lines are fractionation lines corresponding to simple water loss from starting compositions of seawater and serpentine. Errors are 1σ, errors for uncorrected data not shown for clarity. Data sources: fluid inclusions in quartz veins in metapelites (shown in green box) from Besshi, Sanbagawa metamorphic belt (Sumino et al., 2011; Yoshida and Hirajima, 2012), serpentine (Kendrick et al., 2011, 2013), fluids released from serpentine during first stage of stepwise dehydration (Serpentine first breakdown fluids) (Kendrick et al., 2011), and seawater at 0 °C (Bruland and Lohan, 2006; Ozima and Podosek, 2002). (For interpretation of the references to color in this figure legend, the reader is referred to the web version of this article.)

5.4. Subduction of marine sedimentary pore fluid-derived water

5.4.1. Cl/H_2O and $^{36}Ar/H_2O$ ratios of fluid inclusions

The sedimentary pore fluid-like compositions of halogens and noble gases are considered to be preserved during subduction processes. Here, we use new proxies, Cl/H_2O and $^{36}Ar/H_2O$ ratios (Fig. 4, Table 2), to test this contention and to gain further insights into how these volatiles are subducted into the mantle.

The salinity (Cl/H_2O ratio) of the H_2O-rich fluid inclusions has been determined in olivine from the xenolith samples using microthermometry (Ishimaru, unpublished results; Kawamoto et al., 2013). The $^{36}Ar/H_2O$ values are derived using the following relationship:

$$(^{36}Ar/H_2O) = (Cl/H_2O) \times (^{40}Ar^{*}/Cl)_{irradiated,crushed} / (^{40}Ar^{*}/^{36}Ar)_{unirradiated}$$

$$(^{40}Ar^{*}/^{36}Ar)_{measured} = (^{40}Ar/^{36}Ar)_{measured} - (^{40}Ar/^{36}Ar)_{air}$$

In the above equation, $(^{40}Ar^{*}/^{36}Ar)$ of unirradiated samples is preferred because they are considered to be least air-contaminated,

Table 2
Ratios of chlorine, ^{36}Ar and H_2O (in units of mol/mol).

Sample	Cl/H_2O (10^{-2})	$^{36}Ar/H_2O$ (10^{-9})	$Cl/^{36}Ar$ (10^6)
Avacha			
#203 ($n = 11$)	0.60 (29)	15.3 (75)	0.389 (31)
air contamination-corrected		*13.7 (67)*	*0.434 (35)*
#629 ($n = 28$)	0.72 (32)	19.9 (88)	0.365 (32)
air contamination-corrected		*19.0 (84)*	*0.382 (34)*
#729 ($n = 22$)	2.04 (69)	16.2 (56)	1.253 (94)
air contamination-corrected		*16.2 (56)*	*1.253 (97)*
F1 ($n = 42$)	2.6 (15)	3.2 (19)	8.32 (84)
air contamination-corrected		*3.0 (18)*	*8.78 (89)*
Pinatubo			
P3 ($n = 33$)	1.65 (32)	4.7 (12)	3.49 (60)
air contamination-corrected		*3.18 (83)*	*5.20 (89)*
P3 olivine ($n = 33$)	1.65 (32)	2.64 (55)	6.28 (46)
air contamination-corrected		*2.23 (47)*	*7.41 (55)*
Seawater (0 °C)[†]	0.98	1.03	9.57

Errors are given as least significant figures in brackets at a 1σ level of confidence. Italics used for air contamination-corrected data. n: number of analyzed fluid inclusions for salinity determinations (Ishimaru, unpublished results; Kawamoto et al., 2013). Data sources: Cl/H_2O ratios in fluid inclusions (Ishimaru, unpublished results; Kawamoto et al., 2013) and seawater at 0 °C (Bruland and Lohan, 2006; Ozima and Podosek, 2002).

i.e. they were heated at 800 °C prior to crushing without being exposed to air between heating and crushing. Nevertheless, it is apparent from Fig. 3 that some air contamination is present (see earlier discussion in section 5.1). The correlation of $^{22}Ne/^{36}Ar$, $^{84}Kr/^{36}Ar$, and $^{132}Xe/^{36}Ar$ between air and seawater enables the correction of air contamination to ^{36}Ar by fitting the $^{22}Ne/^{36}Ar$ ratios to the seawater value. The air contamination-corrected $^{36}Ar/H_2O$ ratios are listed in Table 2 and shown in Fig. 4.

The range of $^{36}Ar/Cl/H_2O$ obtained from fluid inclusions in a quartz vein in metapelites from the Besshi, Sanbagawa metamorphic belt, is also shown in Fig. 4. The Cl/H_2O and $^{36}Ar/H_2O$ ratios of the fluid inclusions in metapelites are calculated using the same method as for the xenoliths. These fluid inclusions are regarded as representing fluids captured during the prograde path, or near the peak metamorphic stage of subduction (Yoshida and Hirajima, 2012). Halogen and noble gas signatures of these fluid inclusions are also sedimentary pore fluid-like and almost identical to those of the Higashi-akaishi peridotites (Sumino et al., 2010, 2011).

The Cl/H_2O ratios of marine sedimentary pore fluids are expected to be almost identical to those of seawater, because only bromine and iodine are released from organic materials in marine sediment (e.g., Fehn et al., 2006), and we assume $^{36}Ar/H_2O$ ratios of marine sedimentary pore fluids are equivalent to air-saturated seawater.

The Cl/H_2O and $^{36}Ar/H_2O$ ratios of serpentine, the likely carrier of sedimentary pore fluid-derived halogens and noble gases, are calculated from the chlorine and ^{36}Ar concentrations of serpentinites, the degree of serpentinization in each serpentinite (Kendrick et al., 2011, 2013), and using the chemical formula of serpentine (13 wt.% of H_2O). Although the Cl/H_2O and $^{36}Ar/H_2O$ ratios of serpentine show a wide range of values, they are lower than sedimentary pore fluids and the fluid inclusion values analyzed in this study (Fig. 4). The Cl/H_2O and $^{36}Ar/H_2O$ ratios of the fluids released during the first stage of serpentine dehydration increase by an order of magnitude (Fig. 4), however the halogen ratios fractionate during this process towards higher Br/Cl values (Kendrick et al., 2011), which is inconsistent with the values of the fluid inclusions. John et al. (2011) have also argued that the original halogen compositions of serpentine are not preserved during stepwise dehydration.

It is possible that the composition of the slab-derived fluids was modified following release from the slab and prior to being trapped as fluid inclusions in the peridotite studied here. Because of the high diffusivity of hydrogen, any loss of this element from fluid inclusions would increase Cl/H_2O and $^{36}Ar/H_2O$ ratios after the fluids were trapped. However, the ratios in fluid inclusions do not follow H_2O-loss lines from seawater and serpentine (shown as dashed lines in Fig. 4), indicating simple hydrogen-loss cannot account for the Cl/H_2O and $^{36}Ar/H_2O$ ratios of these fluid inclusions. The distinct chemical behavior of Cl, ^{36}Ar, and H_2O means they are comparatively easy to fractionate from each other, more so than halogen and noble gas ratios. The fluid inclusions of the Sanbagawa quartz vein also show high $^{36}Ar/H_2O$ ratios with a range overlapping with those of mantle xenoliths. This may indicate most of the fractionation from an original seawater-like composition took place within the slab during fluid migration, although the fluid inclusions were trapped by mantle minerals at several tens of km above subducting slabs.

5.4.2. Subduction processes of the fluids found in the mantle xenoliths

As shown in Fig. 4, fluid inclusions and serpentine have distinct Cl/H_2O and $^{36}Ar/H_2O$ compositions and if serpentine is the source of the fluids then it is difficult to account for the change in composition during devolatilization. As noted earlier, although the Cl/H_2O and $^{36}Ar/H_2O$ ratios of the fluids released during the first stage of serpentine dehydration increase by an order of magnitude (Fig. 4), this involves halogen fractionation (John et al., 2011; Kendrick et al., 2011) inconsistent with the values present in fluid inclusions. This observation leads us to conclude that an alternative subduction process is required to explain the signatures that are preserved in the fluids. Although some relative enrichment in chlorine and ^{36}Ar are still required, it is apparent that the extent of fractionation from seawater is much less than from serpentine. Such fractionation is most likely to have occurred within the subducting slabs (section 5.4.1).

In conventional subduction models, volatile species are incorporated into hydrous minerals formed in an open system with an essentially infinite water–rock (W/R) ratio. Under these conditions, the chemical composition of dissolved components in the water is at steady state and concentrations of incompatible elements in hydrous minerals, especially noble gases, will be kept low and constant during hydrous mineral formation. In contrast, hydration in a closed system with a very low W/R ratio results in minimal change, not only in noble gas and halogen compositions, but also in the ratios of incompatible elements to water, because all of the water and dissolved species are eventually incorporated into the hydrous mineral unless they reach mineral saturation levels.

Closed system hydration may occur at the slab outer rise, where bending of oceanic plates forms faults. Seawater and/or sedimentary pore fluids are thought to be incorporated into the mantle layer via faults (e.g., Ranero et al., 2003). Faccenda et al. (2009) suggested that subhydrostatic conditions or pressure gradient pumping of water into the mantle occurs in this region, and the injected fluids react with the oceanic crust and mantle surrounding the faults to form hydrous minerals. In this environment, if hydration occurs rapidly due to a low W/R ratio, then the water injected along the faults will be chemically isolated from the external source of sedimentary pore fluid. The fault-related water would effectively be in a closed system and the original Cl/H_2O and $^{36}Ar/H_2O$ ratios of the injected sedimentary pore water will be preserved in the newly formed hydrous minerals. Most of seafloor and forearc serpentine shows low Cl/H_2O and $^{36}Ar/H_2O$ ratios (Fig. 4), however, serpentine with higher ratios than those of sedimentary pore fluids has also been found (Kendrick et al., 2013; Sharp and Barnes, 2004). This indicates that serpentine has enough capacity to incorporate chlorine and ^{36}Ar in order to preserve the original compositions of sedimentary pore fluids in a closed system.

As discussed earlier, serpentine dehydration is a stepwise process accompanied by halogen fractionation. Because the first de-

hydration step occurs at relatively shallow depths, the anhydrous oceanic lithospheric mantle has significant water capacity (e.g., van Keken et al., 2011). At this shallow depth, Wada et al. (2012) argued that the fluids hydrate the ambient anhydrous region of the oceanic lithospheric mantle and that the extent of this hydration process is stronger in locally hydrated slabs, which we assume here. Although some of the fluids released from the shallower sections may escape from the slab, this dehydration–hydration process can be regarded as a closed system operating within the whole of the oceanic lithospheric mantle.

The fluids released from hydrous minerals will interact with surrounding rocks during migration in the slab (e.g., Herms et al., 2012). Although fluids contain relatively abundant halogens and noble gasses compared to the rocks, the fluid composition of these elements may change during fluid–rock interaction processes as the water/rock ratio decreases. In contrast, if the fluid flow is highly channelized (e.g., John et al., 2012), the extent of compositional modification by the fluid–rock interaction will be relatively small. In such environments, the unreactive and incompatible noble gas elemental ratios will be preserved because of their high fluid-mobility and the large contrast in concentration between fluids and rocks. In contrast, the behavior of halogens (especially chlorine) in the fluid may be more complicated because some minerals incorporate halogens leading to halogen fractionation (e.g., Kusebauch et al., 2015). Overall, the halogen data in this study show sedimentary pore fluid-like compositions, however the I/Cl ratios of Avacha fluid inclusions show a relatively large (factor of two) variation and a minor deviation from the sedimentary pore fluid trend (Fig. 3). It is possible that these characteristics reflect the processes occurring during fluid–rock interaction.

When the fluids hydrate the surrounding rocks, the relative amounts of ^{36}Ar, Cl, and H_2O in the fluid are expected vary. Some hydrous phases such as lawsonite and phengite are stable in the subducting slab at sub-arc depth (e.g., van Keken et al., 2011). Noble gases are highly incompatible in mineral phases, thus the rehydration process will consume water but little of the ^{36}Ar, and this can explain the observation that $^{36}Ar/H_2O$ ratios in the fluid inclusions are higher than the seawater value (Fig. 4). Some fluid inclusions show higher $^{36}Ar/H_2O$ ratios than the simple water loss trend at given Cl/H_2O ratios. This indicates that a portion of the halogens were removed from fluids during this hydration process; this is consistent with the water–rock interaction suggested previously to explain the small halogen fractionation observed in the Avacha fluid inclusions.

5.5. Water derived from sedimentary pore fluids and carried by serpentine to the mantle wedge

Some studies have argued that the sources of trace elements and water are decoupled in subduction zone magmas and that the major source of water is serpentine (e.g., Hermann and Green, 2001). Halogen and noble gas signatures found in the peridotites investigated here reveal that serpentine supplies a significant amount of water to the mantle wedge beneath volcanic fronts, and that this water is not strongly decoupled from these two groups of elements. Trace elements, which are depleted in serpentine but enriched in the oceanic crust, are thought to be leached during fluid–rock interaction within slabs (e.g., Herms et al., 2012). High-pressure and high-temperature experiments have shown that the presence of chlorine enhances solubilities of large-ion lithophile elements (LILE) and rare-earth elements (REE) into aqueous fluids (Kawamoto et al., 2014; Keppler, 1996; Tsay et al., 2014) and chlorine-rich slab derived fluids are often invoked to explain the greater enrichment of LILE in arc magmas compared to MORB-source magma (Kawamoto et al., 2014; Keppler, 1996). Moreover, the presence of chlorine can fractionate the ratio of light/heavy REE as observed in arc magmas (Tsay et al., 2014). The subduction model in this study strongly suggests that halogen-bearing aqueous fluids are supplied from subducting slabs into the mantle wedge. The seawater-like noble gases in the convecting mantle (Holland and Ballentine, 2006) can be also explained by deeper subduction and/or involvement of the noble gas signatures observed in this study, to the convecting mantle.

6. Conclusions

The halogen and noble gas signatures of the H_2O-rich fluid inclusions in the peridotites sampled along the volcanic fronts from two subduction zones showing contrasting thermal regimes are similar to those of marine sedimentary pore fluids and serpentinites. This observation suggests that serpentine-derived water supplied to the mantle beneath volcanic fronts has preserved its original halogen and noble gas signatures derived from sedimentary pore fluid during the subduction processes. The measured Cl/H_2O and $^{36}Ar/H_2O$ in the peridotites are higher than those in sedimentary pore fluids and serpentine in oceanic plates. The halogen/noble gas/H_2O systematics are interpreted within a model where water is incorporated into serpentine in a closed system formed along fracture zones developed at the outer rise, where oceanic plates bend prior to entering subduction zones. The closed system is maintained until the final stage of serpentine dehydration due to dehydration–hydration process within the oceanic lithospheric mantle. A portion of the fluids released at the final stage of serpentine dehydration hydrates the overlying slabs, however the sedimentary pore fluid-like halogen and noble gas signatures are preserved due to highly channelized fluid flow. This hydration process results in elevated $^{36}Ar/H_2O$ and Cl/H_2O ratios in the remainder of the aqueous fluids, because of their high incompatibilities in minerals. The fluids are supplied to the mantle wedge beneath volcanic fronts and trapped as fluid inclusions in mantle wedge peridotites.

Acknowledgements

Sampling of rocks from the Pinatubo volcano was made possible through arrangements with the Philippine Institute of Volcanology and Seismology. We thank members of the Radioisotope Center, the University of Tokyo, for providing experimental facilities, and the staff of the Irradiation Experiment Facilities, Institute for Materials Research, Tohoku University, for the neutron irradiation at the JRR-3. Some of JP-1 samples (JP-1 #a and #b) were analyzed by Mr. Takehiko Saito. We also thank Drs. Timm John and Jens Hopp for constructive reviews. This study was supported by the JSPS KAKENHI Grant Numbers 14J09380 (to MK), 20740314, 23340169, and 26287139 (to HS) and by the Sumitomo Foundation No. 100191 and Inamori Foundation (to HS). RB and CJB acknowledge funding from the European Research Council (ERC) grant No: 267692 (NOBLE) and UK NERC grants NE/M000427/1 and NE/G018014/1.

Appendix A. The rock type of JP-1

The original sample of JP-1, which was powdered, homogenized, and distributed as a geochemical reference sample by the Geological Survey of Japan, has been classified as dunite (Imai et al., 1995). Our hand specimen, a fragment of the original JP-1 provided by the Geological Survey of Japan, however, contains considerable amounts of orthopyroxene with minor clinopyroxene (Fig. A.1). Orthopyroxene has been partly altered to talc ± chlorite ± tremolite. The JP-1 fragment is weakly deformed with porphyroclastic to tabular textures (Fig. A.1). Modal amounts of olivine, orthopyroxene, clinopyroxene, and chromian spinel have been determined using

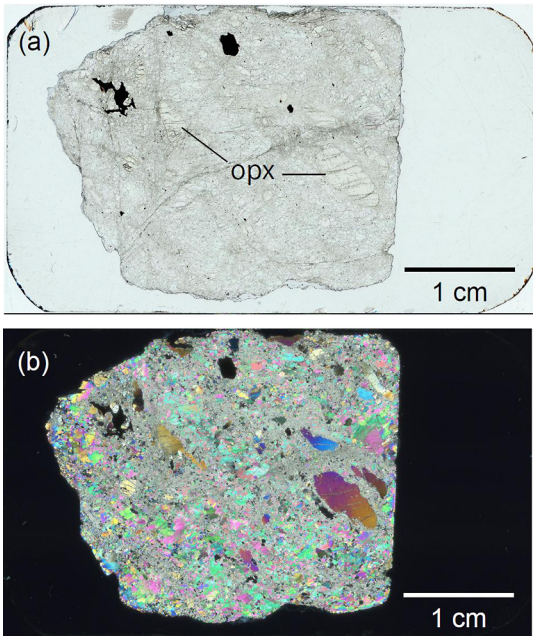

Fig. A.1. Scanned images of the JP-1 fragment. (a) Orthopyroxene (opx) megacrysts (≈1.0 cm) can be observed. Plane-polarized image. (b) Crossed-polarized image of (a).

bulk-rock and mineral compositions (Table A.1). The mineral compositions were determined by FE-SEM (JSM-7001F, JEOL) -EDS (INCA, Oxford Instruments) at Kumamoto University. The calculated modal amount of minerals is Ol: Sp: Opx: Cpx = 76: 1: 21: 2, indicating that JP-1 is more appropriately classified as a harzburgite.

Table A.1
Major element compositions (wt.%) of minerals in a JP-1 fragment.

	Ol	Sp	Opx	Cpx	Amph	JP-1*
SiO_2	39.99		56.55	53.75	56.85	42.38
TiO_2						0.0006
Al_2O_3		21.38	1.31	1.24	0.74	0.66
Cr_2O_3		48.48	0.33	0.42	0.03	0.335
Fe_2O_3		0.70				1.98
FeO	*8.31*	14.15	*5.74*	*1.96*	*2.09*	5.99
MnO		0.00				0.121
MgO	49.75	13.55	34.58	17.93	23.60	44.6
CaO			0.55	23.71	12.11	0.55
Na_2O						0.021
K_2O						0.003
NiO	0.38					0.313
Total	98.43	98.26	99.05	99.00	95.42	96.95
Mg#	0.914	0.630	0.915	0.942	0.953	
Cr#		0.603				

Ol, olivine. Sp, spinel. Opx, orthopyroxene. Cpx, clinopyroxene. Amph, amphibole. Italics indicate, total iron as FeO. Blank, below detection limits. *Recommended or preferable values for major element composition in the geochemical reference material JP-1 (Imai et al., 1995).

Appendix B. Irradiation conditions (Table B.1)

Table B.1
Irradiation conditions.

Irradiation	08HR1	10HR3	10HR5	10HR7
$\Phi_{thermal}$	$(7.26 \pm 0.28) \times 10^{22}$	$(12.80 \pm 0.83) \times 10^{22}$	$(6.49 \pm 0.24) \times 10^{22}$	$(13.14 \pm 0.48) \times 10^{22}$
$\Phi_{thermal}/\Phi_{fast}$	39.1 ± 1.8	40.7 ± 3.3	36.7 ± 2.0	41.2 ± 1.7
$^{38}Ar_{Cl}/Cl$	$(7.61 \pm 0.30) \times 10^{-7}$	$(13.42 \pm 0.87) \times 10^{-7}$	$(6.81 \pm 0.25) \times 10^{-7}$	$(13.78 \pm 0.50) \times 10^{-7}$
$^{80}Kr_{Br}/Br$	$(3.71 \pm 0.14) \times 10^{-5}$	$(6.54 \pm 0.43) \times 10^{-5}$	$(3.32 \pm 0.12) \times 10^{-5}$	$(6.72 \pm 0.25) \times 10^{-5}$
$^{128}Xe_I/I$	$(4.32 \pm 0.17) \times 10^{-5}$	$(7.63 \pm 0.50) \times 10^{-5}$	$(3.87 \pm 0.14) \times 10^{-5}$	$(7.83 \pm 0.29) \times 10^{-5}$
Samples	JP-1 #c, d	Avacha	JP-1 #a, b	Pinatubo, JP-1 #e, f

The calculation methods for these values are described in Johnson et al. (2000), Kendrick (2012), and Ruzié-Hamilton et al. (2016). The units of neutron fluences (Φ) and noble gas production rates from halogen are neutrons/m^2 and mol/mol, respectively. Errors are given at a 1σ level of confidence.

Appendix C. Electron microprobe data of amphibole and silicate glass in Pinatubo and Avacha peridotites

Major elements, fluorine, and chlorine compositions of amphibole and silicate glass were determined by EPMA (JXA8800A, JEOL) at Kanazawa University (Table C.1). Accelerating voltage, probe current, and probe diameter for the analysis were 15 kV, 10 nA, and

Table C.1
Major element, fluorine, and chlorine compositions of amphibole and silicate glass.

	Amphibole										Silicate grass		
	Pinatubo			Avacha							Avacha		
	P3			Av200			Av200 (selvage)		#629		#629		
Abundances in wt.%													
SiO_2	54.86	51.29	46.46	47.46	46.07	45.12	40.65	41.69	46.44	45.79	59.52	61.66	61.22
TiO_2	0.02	0.19	0.33	0.23	0.75	0.61	1.84	1.73	0.26	0.35	0.19	0.17	0.13
Al_2O_3	3.49	7.44	11.55	8.89	11.81	11.50	14.38	13.97	10.94	11.80	20.12	20.31	20.40
Cr_2O_3	0.71	0.95	1.85	1.43	0.05	0.94			0.72	0.83			0.02
FeO*	2.63	3.17	3.56	3.24	4.52	4.27	11.24	11.08	3.71	3.80	2.97	2.44	2.66
MnO	0.03		0.10	0.12	0.15	0.01	0.15	0.17	0.10	0.05	0.03	0.04	0.05
MgO	22.94	20.90	19.15	20.75	19.52	19.30	13.83	14.53	19.78	19.71	2.32	2.16	2.18
CaO	12.35	12.27	12.15	11.30	11.78	11.84	11.88	12.02	11.80	11.78	7.87	7.22	7.29
Na_2O	0.45	1.07	1.78	2.01	2.39	2.32	2.45	2.44	2.22	2.47	5.19	4.89	4.66
K_2O	0.03	0.08	0.11	0.10	0.23	0.20	0.22	0.21	0.26	0.23	0.78	0.90	0.86
NiO	0.09	0.15	0.11	0.04	0.04	0.11			0.16	0.09	0.03	0.05	0.07
Total	97.60	97.51	97.15	95.57	97.31	96.22	96.64	97.84	96.39	96.90	99.02	99.84	99.54
Mg#	0.939	0.922	0.906	0.919	0.885	0.890	0.687	0.700	0.905	0.902	0.582	0.613	0.594
Abundances in ppm													
F													
Cl	135			135				385		288	2173	1346	1385

FeO*, total iron as FeO. Blank, below detection limits (230 ppm for fluorine and 130 ppm for chlorine).

5 μm, respectively. We used JEOL mineral standards (SiO_2, $KTiPO_5$, Al_2O_3, Cr_2O_3, Fe_2SiO_4, MnO, MgO, $CaSiO_3$, $NaAlSi_2O_6$, NiO, CaF, and NaCl) for calibration and counting time for each peak and background were 20 s and 10 s, respectively, except for Ni, Cl (30 s and 15 s, respectively), and P (60 s and 30 s, respectively).

Appendix D. Supplementary material

Supplementary material related to this article can be found online at http://dx.doi.org/10.1016/j.epsl.2016.10.012.

References

Arai, S., Takahashi, N., 1989. Formation and compositional variation of phlogopites in the Horoman peridotite complex, Hokkaido, northern Japan: implications for origin and fractionation of metasomatic fluids in the upper mantle. Contrib. Mineral. Petrol. 101, 165–175.

Arai, S., Ishimaru, S., Okrugin, V.M., 2003. Metasomatized harzburgite xenoliths from Avacha volcano as fragments of mantle wedge of the Kamchatka arc: implication for the metasomatic agent. Isl. Arc 12, 233–246.

Ballentine, C.J., Barfod, D.N., 2000. The origin of air-like noble gases in MORB and OIB. Earth Planet. Sci. Lett. 180, 39–48.

Ballentine, C.J., Holland, G., 2008. What CO_2 well gases tell us about the origin of noble gases in the mantle and their relationship to the atmosphere. Philos. Trans. R. Soc., Math. Phys. Eng. Sci. 366, 4183–4203.

Bolfan-Casanova, N., 2005. Water in the Earth's mantle. Mineral. Mag. 69, 229–257.

Böhlke, J.K., Irwin, J.J., 1992. Laser microprobe analyses of noble gas isotopes and halogens in fluid inclusions: analyses of microstandards and synthetic inclusions in quartz. Geochim. Cosmochim. Acta 56, 187–201.

Briais, A., Patriat, P., Tapponnier, P., 1993. Updated interpretation of magnetic anomalies and seafloor spreading stages in the South China Sea: implications for the Tertiary tectonics of Southeast Asia. J. Geophys. Res., Solid Earth 98, 6299–6328.

Bruland, K.W., Lohan, M.C., 2006. Controls of Trace Metals in Seawater. The Oceans and Marine Geochemistry. Elsevier, pp. 23–47.

Bureau, H., Auzende, A.-L., Marocchi, M., Raepsaet, C., Munsch, P., Testemale, D., Mézouar, M., Kubsky, S., Carrière, M., Ricolleau, A., 2016. Modern and past volcanic degassing of iodine. Geochim. Cosmochim. Acta 173, 114–125.

Bureau, H., Keppler, H., Métrich, N., 2000. Volcanic degassing of bromine and iodine: experimental fluid/melt partitioning data and applications to stratospheric chemistry. Earth Planet. Sci. Lett. 183, 51–60.

Burnard, P., 2004. Diffusive fractionation of noble gases and helium isotopes during mantle melting. Earth Planet. Sci. Lett. 220, 287–295.

Chavrit, D., Burgess, R., Sumino, H., Teagle, D.A.H., Droop, G., Shimizu, A., Ballentine, C.J., 2016. The contribution of the hydrothermal alteration of the ocean crust to the deep halogen and noble gas cycles. Geochim. Cosmochim. Acta 183, 106–124.

Ebisawa, N., Sumino, H., Okazaki, R., Takigami, Y., Hirano, N., Nagao, K., Kaneoka, I., 2004. Construction of I–Xe and ^{40}Ar–^{39}Ar dating system using a modified VG3600 mass spectrometer and the first I–Xe data obtained in Japan. J. Mass Spectrom. Soc. Jpn. 52, 219–229.

Faccenda, M., Gerya, T.V., Burlini, L., 2009. Deep slab hydration induced by bending-related variations in tectonic pressure. Nat. Geosci. 2, 790–793.

Fehn, U., Lu, Z., Tomaru, H., 2006. Data report: $^{129}I/I$ ratios and halogen concentrations in pore water of hydrate ridge and their relevance for the origin of gas hydrates: a progress report. In: Tréhu, A.M., Bohrmann, G., Torres, M.E., Colwell, F.S. (Eds.), Proceedings of the Ocean Drilling Program, Scientific Results, pp. 1–25.

Graham, D.W., 2002. Noble gas isotope geochemistry of mid-ocean ridge and ocean island basalts: characterization of mantle source reservoirs. In: Porcelli, D., Ballentine, C.J., Wieler, R. (Eds.), Noble Gases in Geochemistry and Cosmochemistry. In: Reviews in Mineralogy and Geochemistry, pp. 247–317.

Heber, V.S., Brooker, R.A., Kelley, S.P., Wood, B.J., 2007. Crystal–melt partitioning of noble gases (helium, neon, argon, krypton, and xenon) for olivine and clinopyroxene. Geochim. Cosmochim. Acta 71, 1041–1061.

Hermann, J., Green, D.H., 2001. Experimental constraints on high pressure melting in subducted crust. Earth Planet. Sci. Lett. 188, 149–168.

Herms, P., John, T., Bakker, R.J., Schenk, V., 2012. Evidence for channelized external fluid flow and element transfer in subducting slabs (Raspas Complex, Ecuador). Chem. Geol. 310, 79–96.

Hilton, D.R., Hammerschmidt, K., Teufel, S., Friedrichsen, H., 1993. Helium isotope characteristics of Andean geothermal fluids and lavas. Earth Planet. Sci. Lett. 120, 265–282.

Hirai, H., Arai, S., 1987. H_2O–CO_2 fluids supplied in alpine type peridotites: electron petrology of relic fluid inclusions in olivines. Earth Planet. Sci. Lett. 85, 311–318.

Holland, G., Ballentine, C.J., 2006. Seawater subduction controls the heavy noble gas composition of the mantle. Nature 441, 186–191.

Hopp, J., Ionov, D.A., 2011. Tracing partial melting and subduction-related metasomatism in the Kamchatkan mantle wedge using noble gas compositions. Earth Planet. Sci. Lett. 302, 121–131.

Ikeda, Y., Nagao, K., Kagami, H., 2001. Effects of recycled materials involved in a mantle source beneath the southwest Japan arc region: evidence from noble gas, Sr, and Nd isotopic systematics. Chem. Geol. 175, 509–522.

Imai, N., Terashima, S., Itoh, S., Ando, A., 1995. 1994 compilation of analytical data for minor and trace elements in seventeen GSJ geochemical reference samples, "igneous rock series". Geostand. Newsl. 19, 135–213.

Ishimaru, S., Arai, S., 2009. Highly silicic glasses in peridotite xenoliths from Avacha volcano, Kamchatka arc; implications for melting and metasomatism within the sub-arc mantle. Lithos 107, 93–106.

Ishimaru, S., Arai, S., Ishida, Y., Shirasaka, M., Okrugin, V.M., 2007. Melting and multi-stage metasomatism in the mantle wedge beneath a frontal arc inferred from highly depleted peridotite xenoliths from the Avacha volcano, Southern Kamchatka. J. Petrol. 48, 395–433.

Iwamori, H., 2007. Transportation of H_2O beneath the Japan arcs and its implications for global water circulation. Chem. Geol. 239, 182–198.

Jarrard, R.D., 2003. Subduction fluxes of water, carbon dioxide, chlorine, and potassium. Geochem. Geophys. Geosyst. 4, 8905.

John, T., Gussone, N., Podladchikov, Y.Y., Bebout, G.E., Dohmen, R., Halama, R., Klemd, R., Magna, T., Seitz, H.-M., 2012. Volcanic arcs fed by rapid pulsed fluid flow through subducting slabs. Nat. Geosci. 5, 489–492.

John, T., Layne, G.D., Haase, K.M., Barnes, J.D., 2010. Chlorine isotope evidence for crustal recycling into the Earth's mantle. Earth Planet. Sci. Lett. 298, 175–182.

John, T., Scambelluri, M., Frische, M., Barnes, J.D., Bach, W., 2011. Dehydration of subducting serpentinite: implications for halogen mobility in subduction zones and the deep halogen cycle. Earth Planet. Sci. Lett. 308, 65–76.

Johnson, L.H., Burgess, R., Turner, G., Harris, J.W., 2000. Noble gas and halogen geochemistry of mantle fluids: comparison of African and Canadian diamonds. Geochim. Cosmochim. Acta 64, 717–732.

Kawamoto, T., Mibe, K., Bureau, H., Reguer, S., Mocuta, C., Kubsky, S., Thiaudière, D., Ono, S., Kogiso, T., 2014. Large-ion lithophile elements delivered by saline fluids to the sub-arc mantle. Earth Planets Space 66, 1–11.

Kawamoto, T., Nakajima, J., Reynard, B., Toh, H., 2015. In: Special issue 'Geofluid processes in subduction zones and mantle dynamics'. Earth Planets Space 67, 1–4.

Kawamoto, T., Yoshikawa, M., Kumagai, Y., Mirabueno, M.H.T., Okuno, M., Kobayashi, T., 2013. Mantle wedge infiltrated with saline fluids from dehydration and decarbonation of subducting slab. Proc. Natl. Acad. Sci. 110, 9663–9668.

Kendrick, M.A., 2012. High precision Cl, Br and I determinations in mineral standards using the noble gas method. Chem. Geol. 292–293, 116–126.

Kendrick, M.A., Kamenetsky, V.S., Phillips, D., Honda, M., 2012. Halogen systematics (Cl, Br, I) in Mid-Ocean Ridge Basalts: a Macquarie Island case study. Geochim. Cosmochim. Acta 81, 82–93.

Kendrick, M.A., Honda, M., Pettke, T., Scambelluri, M., Phillips, D., Giuliani, A., 2013. Subduction zone fluxes of halogens and noble gases in seafloor and forearc serpentinites. Earth Planet. Sci. Lett. 365, 86–96.

Kendrick, M.A., Honda, M., Vanko, D.A., 2015. Halogens and noble gases in Mathematician Ridge meta-gabbros, NE Pacific: implications for oceanic hydrothermal root zones and global volatile cycles. Contrib. Mineral. Petrol. 170, 1–20.

Kendrick, M.A., Scambelluri, M., Honda, M., Phillips, D., 2011. High abundances of noble gas and chlorine delivered to the mantle by serpentinite subduction. Nat. Geosci. 4, 807–812.

Keppler, H., 1996. Constraints from partitioning experiments on the composition of subduction-zone fluids. Nature 380, 237–240.

Kurz, M.D., 1986. Cosmogenic helium in a terrestrial igneous rock. Nature 320, 435–439.

Kusebauch, C., John, T., Barnes, J.D., Klügel, A., Austrheim, H.O., 2015. Halogen element and stable chlorine isotope fractionation caused by fluid–rock interaction (Bamble Sector, SE Norway). J. Petrol. 56 (2), 299–324.

Matsuda, J., Nagao, K., 1986. Noble-gas abundances in a deep-sea sediment core from Eastern Equatorial Pacific. Geochem. J. 20, 71–80.

Matsumoto, T., Chen, Y.L., Matsuda, J., 2001. Concomitant occurrence of primordial and recycled noble gases in the Earth's mantle. Earth Planet. Sci. Lett. 185, 35–47.

Minster, J.B., Jordan, T.H., Molnar, P., Haines, E., 1974. Numerical modelling of instantaneous plate tectonics. Geophys. J. Int. 36, 541–576.

Mitsui, Y., Hirahara, K., 2009. Coseismic thermal pressurization can notably prolong earthquake recurrence intervals on weak rate and state friction faults: numerical experiments using different constitutive equations. J. Geophys. Res., Solid Earth, 114.

Miura, Y., Nagao, K., 1991. Noble-gases in 6 GSJ igneous rock samples. Geochem. J. 25, 163–171.

Ozima, M., Podosek, F.A., 2002. Noble Gas Geochemistry. Cambridge University Press.

Porcelli, D., Ballentine, C.J., 2002. Models for distribution of terrestrial noble gases and evolution of the atmosphere. In: Porcelli, D., Ballentine, C.J., Wieler, R. (Eds.), Noble Gases in Geochemistry and Cosmochemistry. In: Reviews in Mineralogy and Geochemistry, pp. 411–480.

Ranero, C.R., Morgan, J.P., McIntosh, K., Reichert, C., 2003. Bending-related faulting and mantle serpentinization at the Middle America trench. Nature 425, 367–373.

Ruzié-Hamilton, L., Clay, P.L., Burgess, R., Joachim, B., Ballentine, C.J., Turner, G., 2016. Determination of halogen abundances in terrestrial and extraterrestrial samples by the analysis of noble gases produced by neutron irradiation. Chem. Geol. 437, 77–87.

Sharp, Z.D., Barnes, J.D., 2004. Water-soluble chlorides in massive seafloor serpentinites: a source of chloride in subduction zones. Earth Planet. Sci. Lett. 226, 243–254.

Staudacher, T., Allègre, C.J., 1988. Recycling of oceanic-crust and sediments – the noble-gas subduction barrier. Earth Planet. Sci. Lett. 89, 173–183.

Sumino, H., Ballentine, C.J., Burgess, R., Endo, S., Yoshida, K., Mizukami, T., Holland, G., Wallis, S.R., Hirajima, T., 2011. Slab-derived halogens and noble gases with a marine pore-fluid signature. Mineral. Mag. 75, 1963.

Sumino, H., Burgess, R., Mizukami, T., Wallis, S.R., Holland, G., Ballentine, C.J., 2010. Seawater-derived noble gases and halogens preserved in exhumed mantle wedge peridotite. Earth Planet. Sci. Lett. 294, 163–172.

Sumino, H., Nagao, K., Notsu, K., 2001. Highly sensitive and precise measurement of helium isotopes using a mass spectrometer with double collector system. J. Mass Spectrom. Soc. Jpn. 49, 61–68.

Takahashi, N., 1992. Evidence for melt segregation towards fractures in the Horoman mantle peridotite complex. Nature 359, 52–55.

Tatsumi, Y., 1989. Migration of fluid phases and genesis of basalt magmas in subduction zones. J. Geophys. Res. 94, 4697–4707.

Tsay, A., Zajacz, Z., Sanchez-Valle, C., 2014. Efficient mobilization and fractionation of rare-earth elements by aqueous fluids upon slab dehydration. Earth Planet. Sci. Lett. 398, 101–112.

Turner, G., 1965. Extinct iodine 129 and trace elements in chondrites. J. Geophys. Res. 70, 5433–5445.

van Keken, P.E., Hacker, B.R., Syracuse, E.M., Abers, G.A., 2011. Subduction factory: 4. Depth-dependent flux of H_2O from subducting slabs worldwide. J. Geophys. Res., Solid Earth 116, B01401.

Wada, I., Behn, M.D., Shaw, A.M., 2012. Effects of heterogeneous hydration in the incoming plate, slab rehydration, and mantle wedge hydration on slab-derived H_2O flux in subduction zones. Earth Planet. Sci. Lett. 353–354, 60–71.

Yamamoto, J., Nishimura, K., Sugimoto, T., Takemura, K., Takahata, N., Sano, Y., 2009. Diffusive fractionation of noble gases in mantle with magma channels: origin of low He/Ar in mantle-derived rocks. Earth Planet. Sci. Lett. 280, 167–174.

Yoshida, K., Hirajima, T., 2012. Annular fluid inclusions from a quartz vein intercalated with metapelites from the Besshi area of the Sanbagawa belt, SW Japan. J. Mineral. Petrol. Sci. 107, 50–55.

Yoshikawa, M., Nakamura, E., 2000. Geochemical evolution of the Horoman peridotite complex: implications for melt extraction, metasomatism, and compositional layering in the mantle. J. Geophys. Res., Solid Earth 105, 2879–2901.

Yoshikawa, M., Tamura, A., Arai, S., Kawamoto, T., Payot, B.D., Rivera, D.J., Bariso, E.B., Mirabueno, M.H.T., Okuno, M., Kobayashi, T., 2016. Aqueous fluids and sedimentary melts as agents for mantle wedge metasomatism, as inferred from peridotite xenoliths at Pinatubo and Iraya volcanoes, Luzon arc, Philippines. Lithos 262, 355–368.